Visualization of supersonic free and confined jet using planar laser mie scattering technique

Article *in* Journal of the Indian Institute of Science · March 2016

CITATIONS
8

READS
3,515

3 authors:

Sengunthapuram Kandasamy Karthick
Technion - Israel Institute of Technology
55 PUBLICATIONS **205** CITATIONS
SEE PROFILE

Jagadeesh Gopalan
Indian Institute of Science
297 PUBLICATIONS **2,320** CITATIONS
SEE PROFILE

K P J Reddy
Indian Institute of Science
268 PUBLICATIONS **1,972** CITATIONS
SEE PROFILE

Journal of the Indian Institute of Science
A Multidisciplinary Reviews Journal
ISSN: 0970-4140 Coden-JIISAD

REVIEWS

Visualization of Supersonic Free and Confined Jet using Planar Laser Mie Scattering Technique

S.K. Karthick, G. Jagadeesh and K.P.J. Reddy*

Abstract | Planar Laser Mie Scattering (PLMS) imaging technique is employed in supersonic axisymmetric free jet and supersonic rectangular confined jet to extract out the prominent flow features. Efficient seeding of the flow field is achieved using an in-house seeder unit which employs modified Laskin Nozzle. For this imaging, flow field is seeded with particles of water or DEHS in case of free jet studies and with acetone for confined jet studies. Using high power laser and high speed camera, flow field is illuminated and captured. A series of simple image processing routines are carried out to extract the noticeable attributes of the flow. Prominent flow features like Mach disc, shear layer instability and shock cells are captured in the instantaneous PLMS images of a severely under-expanded supersonic axisymmetric free jet of design Mach number (M_D) 1.367. Qualitative increase in the shock cell spacing (L_s) for increasing Mach number ratio (M_R) is observed for time-averaged PLMS imaging of a supersonic axisymmetric free jet (M_D = 2.0 & 2.5). Also an effective increase in the jet width of an over-expanded jet undergoing screech is noticed. Major flow features like large scale coherent structures and terminal potential core instability are seen clearly in the instantaneous PLMS images of a rectangular supersonic confined jet of M_{PD} = 2.0. Shock cell spacing and mixing layer formation are observed distinctly in the time-averaged PLMS images. Qualitative increase in L_s for increasing stagnation pressure ratio (SPR) is highlighted along with the increase in the wavelength of the potential core instability. More details regarding the experimentation procedure and the underlying physics behind the observed flow features along with the variations encountered for different operating conditions are discussed elaborately in this paper.

Keywords: *PLMS, Supersonic Free Jet, Supersonic Confined Jet, Visualization Techniques*

1 Introduction

Visualization of flow fields are of paramount importance in reasoning the physics behind it. Qualitative visualization tools like smoke visualization,[1] tuft-grid visualization,[2] surface oil flow visualization[3] and shadowgraph & Schlieren[4] techniques are frequently used to access the incompressible and compressible gaseous flow field. Each technique has its own advantage and disadvantage over one another. When it comes to compressible gaseous flow field, surface oil flow visualizations are preferred in wall shear flows to get information happening near the wall. For free shear flows, mostly shadowgraph & Schlieren techniques are employed. Instantaneous flow imaging is impossible in surface oil flow visualizations as the flow field is marked by the formation of streak-lines. Shadowgraph & Schlieren techniques are based upon the line of sight integrated density variation imaging procedure, which helps in getting instantaneous images, but lacks in providing fine details that

Laboratory for Hypersonic and Shock-wave Research, Department of Aerospace Engineering, Indian Institute of Science, Bangalore, India.
**skkarthick@ymail.com*

happen inside the flow field, especially when the flow is three dimensional. In recent decades, laser scattering methods[5] are very popular among experimental aerodynamicist. A converted high power laser beam of visible wavelength into a sheet of desired dimensions with a thickness of 1 mm, slices the flow field and helps in visualizing the fluid structures (provided the flow-field is sufficiently seeded so that the laser light can be scattered). Usage of continuous laser light source and a high speed camera for imaging helps in capturing structures that evolves in both space and time, particularly at low speeds. In high speed flows, pulsating laser with a pulse width of about 10 ns along with a laser pulse synced camera are used to capture crisp flow features in space. But temporal evolutions of such structures are difficult to capture, as the repetition rate of those lasers are in the order of few hertz (Hz). In modern days, development of high speed lasers having a repetition rate ranging from kHz to MHz helps in overcoming the difficulty of temporal evolution of flow structures. Although these higher end lasers are nowadays used in several other methods to quantify flow field variables like in high speed PIV,[6,7] PLIF[8] etc., it can also be used as a qualitative tool. Just by going through a simple laser scattering image itself, many qualitative features of the flow can be identified. Laser scattering can happen in two regimes: a. Rayleigh and b. Mie. When the wavelength of the incident laser light sheet is larger than the scattering particles itself, then the scattering happens in the Rayleigh regime and is called as Planar Laser Rayleigh Scattering (PLRS). If the wavelength of the incident laser light sheet is lesser than the scattering particles itself, then the scattering happens in Mie regime, called the Planar Laser Mie Scattering (PLMS). Producing and seeding larger particles in the flow field are simpler than producing and seeding smaller particles in the flow field. Hence, many of the researchers prefer Mie over Rayleigh scattering for qualitative visualizations. A typical scattering pattern observed in PLMS is depicted in Figure 1.

PLMS studies are initially attempted in mixing layers using small alcohol droplets.[5] Later, this technique is employed in exploring 2D[9] & 3D[10] effects and large scale structures[11] in supersonic planar mixing layers. Most of the supersonic mixing studies in combustion related works like swept ramp fuel injection,[12] single port & twin port injection,[13] H_2 jet injection,[14] strut based injection[15] and fin-guided fuel injection[16] use PLMS technique as a primary investigation tool. PLMS technique is frequently used in the study of supersonic streamwise[17–22] and transverse[23–28] jet analysis. In recent decades, mixing enhancement[29–33] studies, both in open and closed domain flows are very often carried out through PLMS techniques. Lately, studies on supersonic ejector[34–37] or supersonic jet in confinement[38–41] are using PLMS technique for quantifying mixing and other flow features. Although, this technique is in usage for the last 25 years, a clear usage of these techniques, especially for supersonic jet flows are not clearly available in literature. With the development in laser technology, high speed imaging camera and digital image processing techniques, PLMS technique can provide deeper insights to the flow physics. This paper is written to emphasize the usage of Planar Laser Mie Scattering (PLMS) method to visualize high speed supersonic jets using recently developed high speed laser, imaging and acquisition systems. Major part of this paper is dedicated to the process of selection, production and use of particles for PLMS experiments. Detailed insights are given in designing a particle seeder unit to handle large flow rate requirements. A thorough image processing routine is highlighted to get a crispy

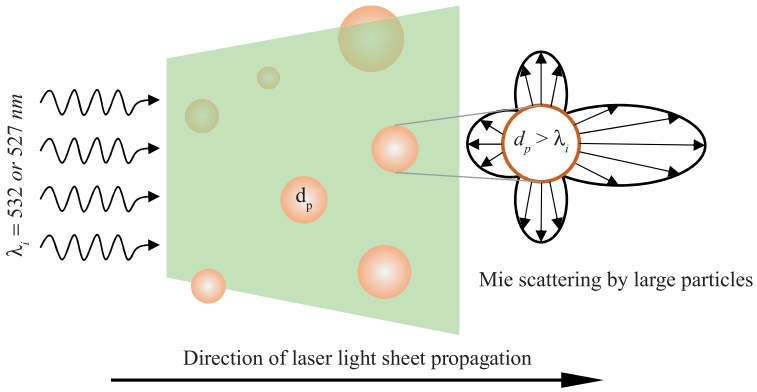

Figure 1: Typical scattering pattern observed in PLMS technique.

flow image from a raw camera image. High speed supersonic axisymmetric free jet and a supersonic rectangular confined jet are considered here for the PLMS visualization. Along with the brief introduction about the visualization technique in current section, this paper is divided into four major sections. In the second section, detailed experimental methodology along with the facility description for the simulation of supersonic free and confined jet, details about flow seeding and imaging procedures are described. In the third section, observed flow features in supersonic free and confined jet are discussed elaborately. Fourth section carries the major conclusion of PLMS visualization in the considered high speed jet studies.

2 Experimental Methodology

2.1 *Facility*

2.1.1 Blow-down facility: Air is compressed by the ELGI™ (E22–13 GS) Screw Compressor of 30 HP having 95 CFM with a maximum operating pressure of 12.5 bar. The entire compressor unit is controlled by a separate module called Variable Frequency Drives (ELGI™ VFD) for low power consumption and also to eliminate the frequent load-unload cycle. It has added mechanical advantages, like minimum maintenance, smooth start and smooth control. The compressed air is then passed through ELGI™ Airmate Refrigerant Air Dryer (ELRD 150). When flow expands through the nozzle, the temperature will be very low, and as a result of it water vapor precipitates as condensate. In order to avoid such happenings efficient dryer is required. Between the inlet and outlet of the dryer, a high efficiency oil removal filtration unit is used. ELGI™ Airmate Economy Series Filters are used in this facility (FF-E-0125). These units are used for the removal of particles down to 0.01 micron including water and oil aerosols, providing a maximum remaining oil aerosol content of 0.01 mg/m^3 at 21°C. After the air treatment, the compressed air is stored in the ELGI™ Receivers. The facility has 3 number of air receivers. Two of them are of 3 m^3 and one of them is of 1 m^3, by storage volume. The maximum working pressure of those air receivers is 12.5 bar. A 2" pipeline is used to draw the air from the receivers, and a simple gate valve to feed the air in to the pressure regulator. SHAVO™ pressure regulator is used to set an operating pressure of 3 to 10 bar, NISHANKA™ Pneumatic Rotary Actuator to start the tunnel using simple hand operated switch. A long chamber of 200 mm diameter is made used of as a stagnation chamber and the stagnation pressure of the primary flow (P_{op}) is measured.

2.1.2 Supersonic free jet: At the end of the stagnation chamber, after measuring the stagnation pressure, flow is accelerated through a convergent section smoothly to the conical nozzle entry. Externally convergent and internally convergent-divergent nozzle is attached at the end of the convergent section, which is used to accelerate the flow to supersonic speeds. A typical layout of the supersonic free jet testing facility is shown in Figure 2. Internal dimensions of the nozzle that is used for PLMS experiments are shown in Figure 3.

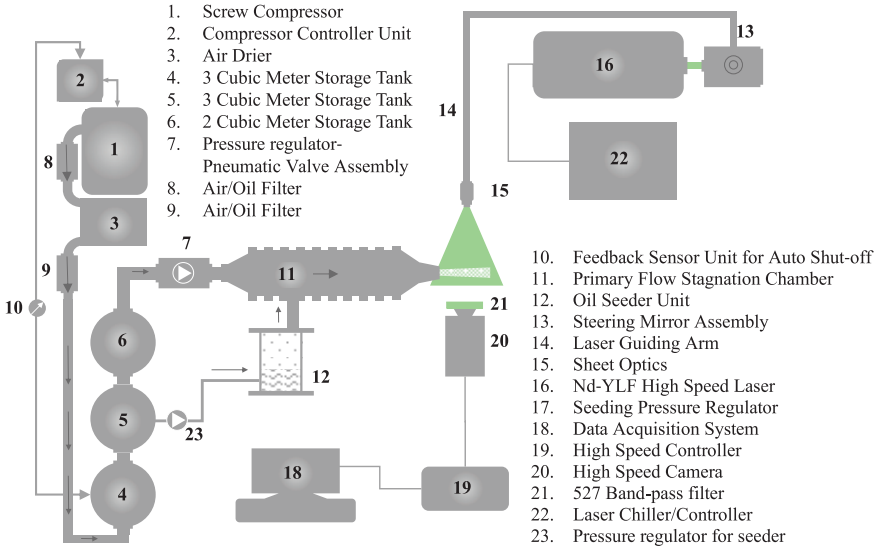

Figure 2: A typical layout of the supersonic free jet testing facility.

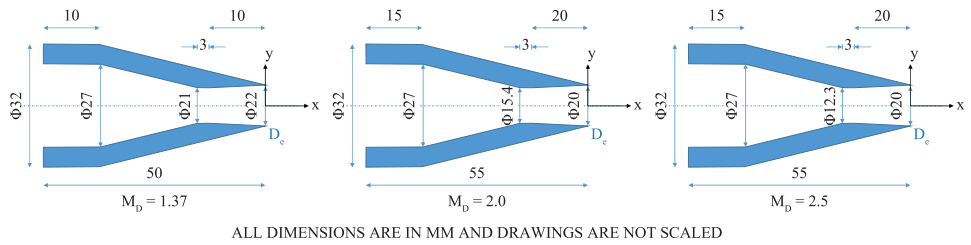

Figure 3: Internal dimensions of the conical CD nozzle used in supersonic free jet PLMS experiments.

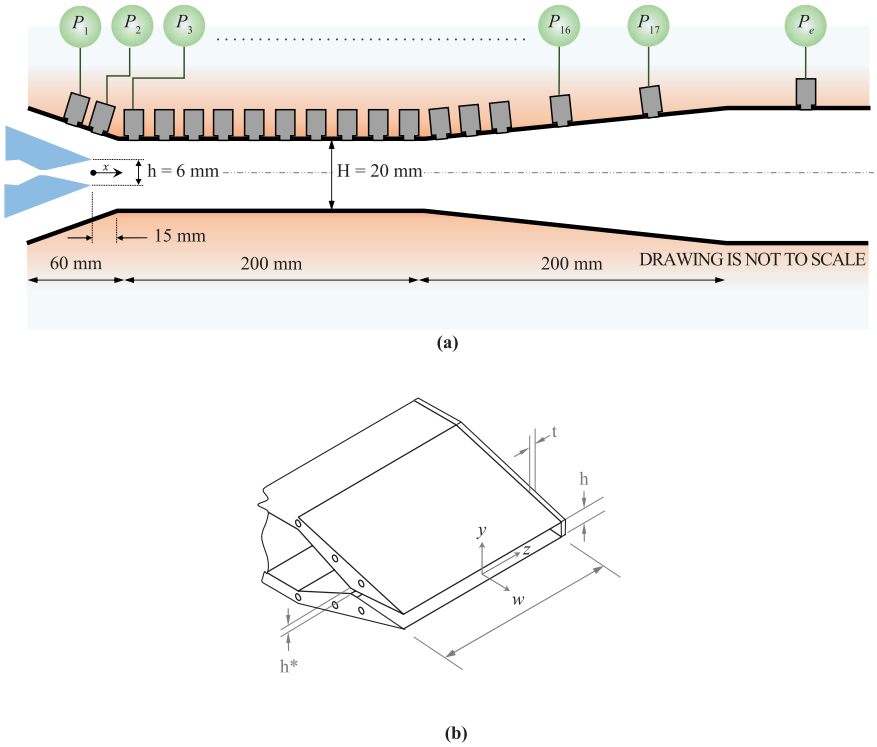

Figure 4: (a) Flow passage dimensions of the supersonic closed jet or supersonic gaseous ejector (drawn not to scale); (b) Dimensions of the primary flow CD nozzle (h = 6 mm, t = 2 mm, w = 75 mm & for M_{PD} = 2.0, h* = 3.6 mm).

2.1.3 Supersonic confined jet: In the same blow-down facility, at the end of the stagnation chamber, flow is gradually accelerated through a convergent section, followed by a rectangular nozzle of large aspect ratio (AR = 12.5). Similar to the conical nozzle, this rectangular nozzle is also externally convergent and internally convergent-divergent, to accelerate the flow to supersonic speeds. This rectangular nozzle is inserted into a confinement, which consists of three parts: a. Converging section, b. Constant area mixing duct, and c. Diffuser. Because of the primary flow expanding through the rectangular nozzle at high kinetic energy, due to local pressure drop, secondary flow is sucked into the confinement through the converging section. In order to meter the flow, venturi-meter is connected at the secondary flow air intake duct. Mixing duct is enclosed by BK-7 glass windows on either sides to access the flow optically. Entrained secondary flow and primary flow undergo turbulent mixing in the mixing duct and exit through the diffuser. One more viewing window is given near the diffuser end for optical access. After the exit of the flow through the diffuser, exhaust piping is done to take the flow outside. More details about the facility rigging and ejector dimensions are given in Ref [34]. Basic dimensions of the ejector module and the primary flow nozzle are given in Figure 4.

2.2 *PLMS visualization*

2.2.1 High energy laser: High energy laser light source is important for achieve better scattering in PLMS experiments. Two types of laser are used in

our experiments. A low speed (10 Hz), small pulse width (10 ns), Nd-YAG laser (500 mJ) at 532 nm is used for supersonic free jet studies and a high speed (0.1–10 kHz), medium pulse width (100 ns), Nd-YLF laser (24 mJ) at 527 nm is used for supersonic confined jet studies. Both the lasers are having a beam width around 8 mm and they are transported to the field of investigation through a 1.6 m laser guiding arm. An appropriate sheet making optics is used to convert the laser beam into a laser sheet of thickness around 0.5 mm. Some important features of the laser that are mentioned above helps in visualizing particular flow aspects and the details will be discussed in the upcoming sections.

2.2.2 Imaging & acquisition: A Phantom Miro 110 high speed camera (1280 pixel × 800 pixel, 20 μm/pixel) is used to capture scattering images at a minimum exposure of 2 μs and a maximum frame rate of 1600 fps. Recording rate of the camera is fixed on the basis of the laser that is used along with it. A High Speed Control (HSC) unit is used to sync the laser pulse and the camera frame. A Nikon 40 mm f/2.8 G micro lens is used to capture the images. Basic imaging module in Davis 8.3 is used as an interfacing software for capturing PLMS images and to control HSC. Images are acquired through a camera having 527 ± 5 nm band pass filter to avoid unwanted reflections. For higher signal to noise ratio (SNR) in the captured Mie scattering image, Scheimpflug imaging technique is used to look at the planar sheet at an oblique angle, since the Mie scattering will be dominant in the forward lobe (Figure 1). Rigorous image processing has been carried out then to eliminate camera noise, parasite reflections and image distortions through the software. A typical timing diagram to acquire PLMS images using a laser pulse and a camera with a filter is given in Figure 5.

2.2.3 Seeding system: Particles can be formed at lower density in the form of few clusters or it can be formed at higher density in the form of heavy clouds. Hydrated air upon condensation forms particle clouds which seed the flow. Production of distinct particles using particle generators form particle clusters and seed the flow. To produce particle clouds from hydrated air, compressed air is stored without using a dryer. To produce particles of size larger than the wavelength of the incident light source, a modified Laskin nozzle particle generator is designed in-house to meet the larger mass flow through the supersonic nozzle. A schematic of the single modified Laskin particle seeder module is given in Figure 6(a). Front view and isometric view with a cut section of the designed particle seeder unit with nine modules of modified Laskin generator is shown in Figure 6(b). Air has been passed through the top portion of the strut and it exits through 11 circular holes, each of diameter 0.8 mm, lying on the periphery, near the sealed bottom of the strut. Portion of the strut carrying the nozzle around the periphery is immersed in the fluid that is about to be nebulized. Critical height has to be maintained, as the number density of the particles being produced depends on it. Air exhausting through the nozzles that are immersed in the fluid is choked at the exit and expands further in the fluid. High speed air jet expanding in the liquid, shears and entrains fluid particles in it in the form of bubbles. These bubbles burst and produce fine particles while convecting downstream towards the liquid surface. Each strut is isolated from the other struts using an isolation chamber. Liquid splashing is avoided

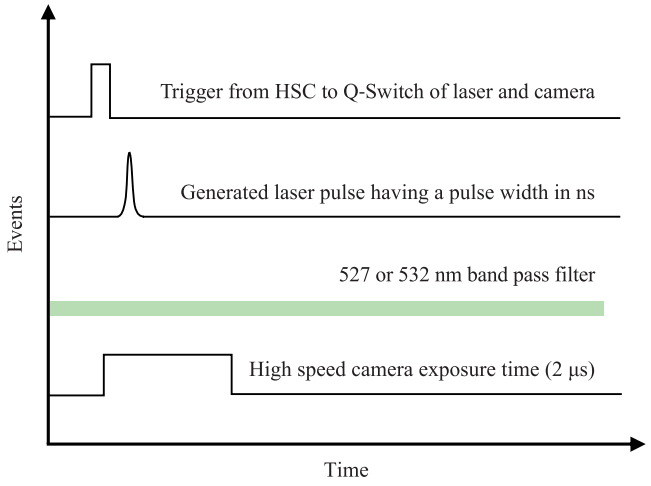

Figure 5: A typical timing diagram to acquire PLMS images using a laser pulse and a camera with a filter.

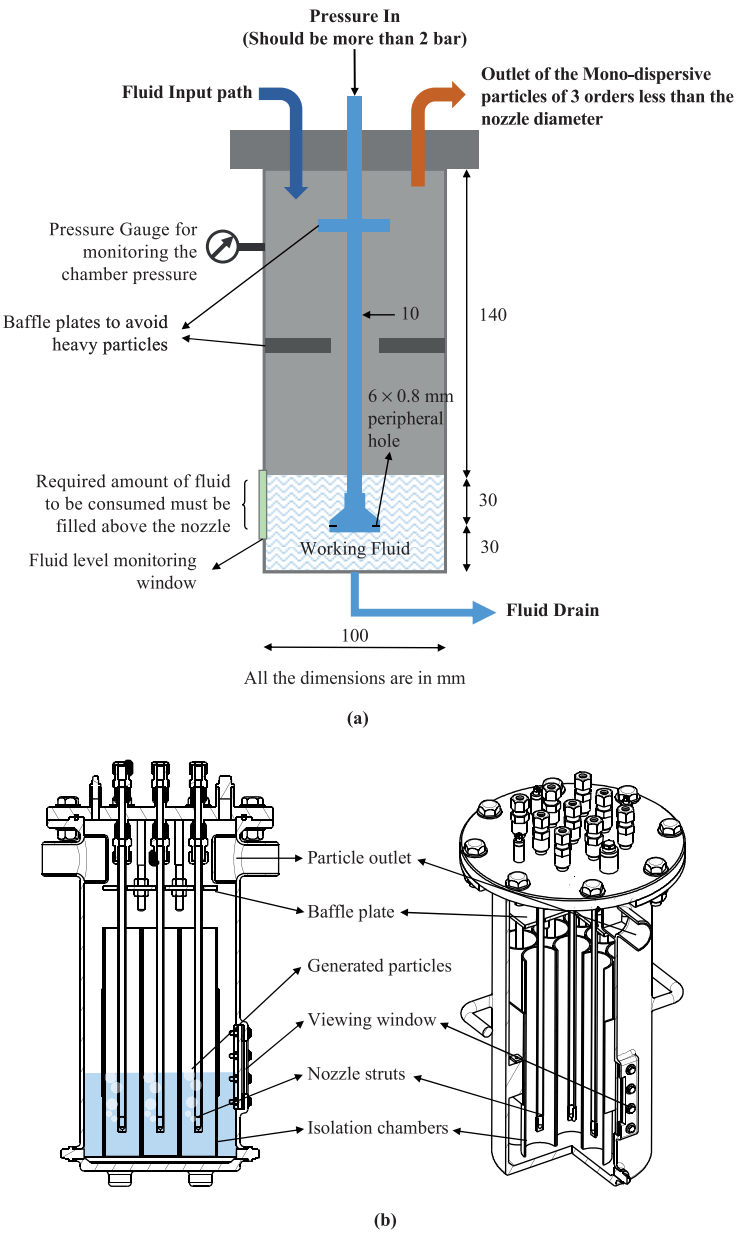

Figure 6: (a) Schematic of the single modified Laskin particle seeder module (b) Front view and isometric view with a cut section of the designed particle seeder unit with nine modules of modified Laskin generator.

by placing a splash plate some distance away from the liquid surface. Various fluids are identified as potential candidates to produce particles of required diameter. Smoke is ruled out due to the fact that it cannot be pumped into the stagnation chamber at pressure above atmospheric. Other fluids like water, acetone, refined sunflower oil and DEHS (Di-ethyl glycol compound or 'Smoke Fluid 'P') are tried out. Particle size distribution studies are carried out using a Phase Doppler Particle Analyzer (PDPA) and Wide Range Particle Spectrometer (WRPS) under standard conditions. Typical particle size distribution curves observed for various fluids are given in Figure 7. Acetone is found to be a suitable candidate for confined flow studies as it self-cleans the viewing windows. For free jet studies, water or DEHS fluid is used. Hydrated air is sometimes useful in visualizing flow field as the air condense and forms particle clouds when the flow expands through the nozzle (case of $\Delta P = 0$ in Figure 8). For a particle size of 0.6–1.2 μm, particle response time is calculated as 0.8–3.0 μs which ensures that the particles are following the fluid flow faithfully. Enough particles are pumped into the stagnation chamber by maintaining a differential pressure (ΔP) of 2

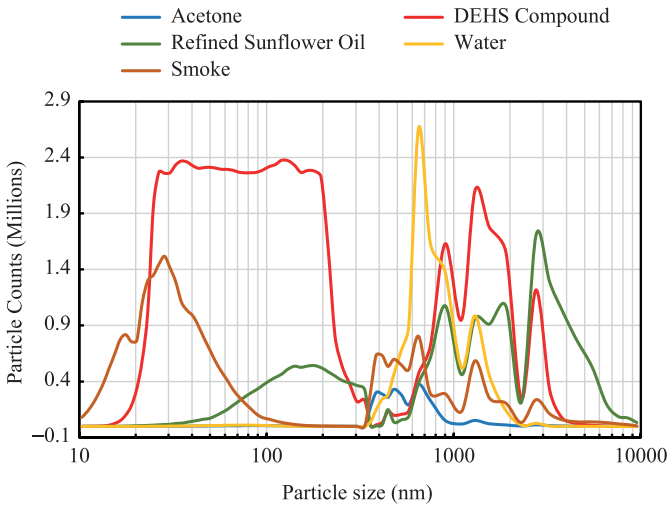

Figure 7: Particle size distribution chart for various fluids using PDPA & WRPS measurements.

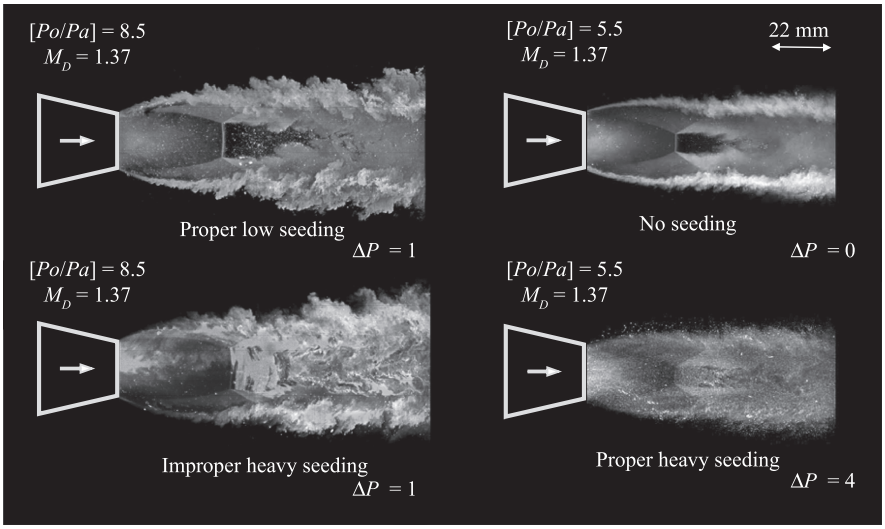

Figure 8: Influence of differential pressure and particle mixing in PLMS imaging technique.

bar between the seeder unit and the stagnation chamber. Level of seeding can be controlled by maintaining this differential pressure. Particles are injected in opposite directions into the stagnation chamber in order to promote particle mixing with the main flow. Influence of differential pressure and particle mixing are clearly highlighted in Figure 8. Required particle concentration is selected based upon the flow field under study.

2.2.4 Image processing techniques: Acquired PLMS raw images contain noise, parasite reflections and background stray reflections. Though the band pass filter (that we use along with the camera) helps in reducing most part of the reflections, a set of image processing is mandatory to get a crispy image. With the laser sheet illuminating the investigating area without the flow field, few images are taken as reference image for subtraction operation. Similarly, a uniform seeding is done on the flow field and images are taken to analyze the intensity variation observed in the laser sheet. This process helps in avoiding the accumulated laser energy in the middle part of the laser sheet. Once these pre-processing techniques are done, images are taken with flow. All the acquired flow images are subtracted from the reference background image to get a higher SNR. After that, those images should be corrected for the laser sheet intensity variations. At last, all the processed images are subjected to image sharpening process to get enhanced flow structures. In Figure 9, image processing routines that are carried out in PLMS imaging technique are illustrated in order.

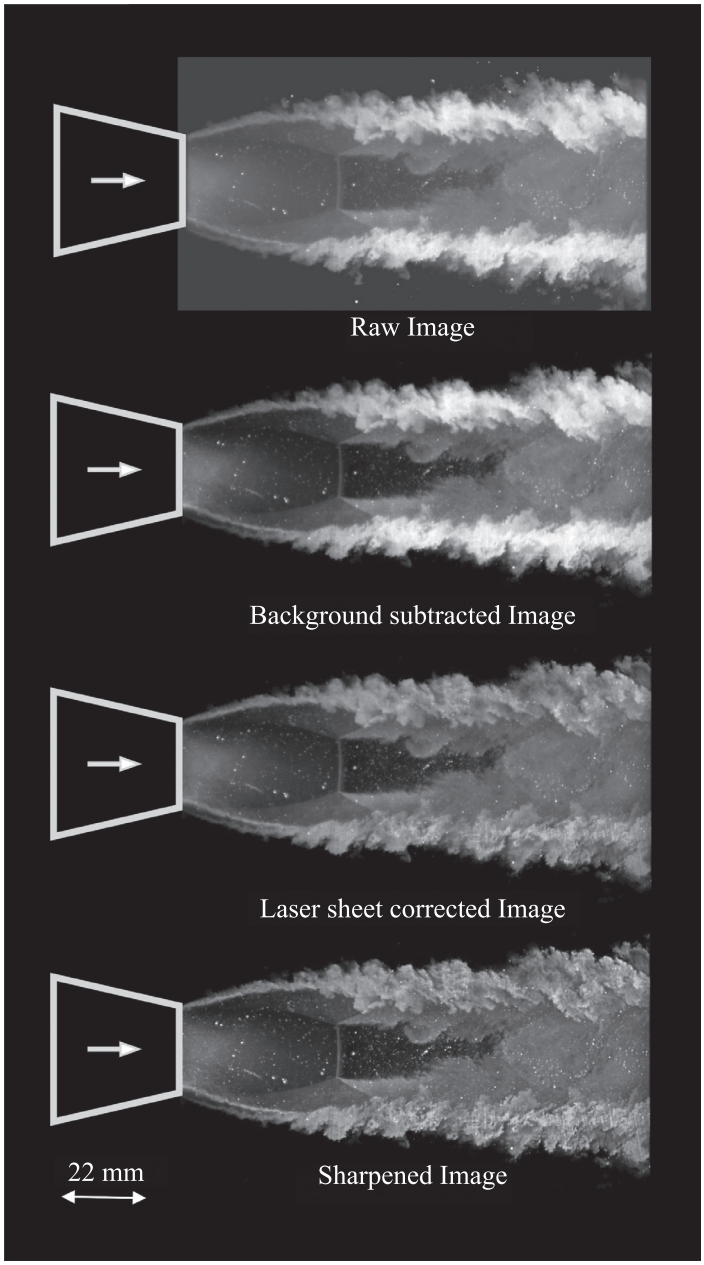

Figure 9: Image processing routine in PLMS imaging technique (Conditions: P_o/P_a = 8.5, M_D = 1.37, moderate seeding).

3 Observations and Discussions

3.1 *Supersonic free jet*

3.1.1 Prominent flow features in a supersonic axisymmetric free jet (M_D = 1.37): PLMS imaging of supersonic free jet of design Mach number 1.37 expanding at a total pressure of 7 bar is captured using Nd-YAG laser at 10 Hz. Instantaneous and time-averaged PLMS images are given in Figure 10 & 11. Flow coming out from left to right under such condition produces a strong Mach disc that stands nearly 0.75D from the exit of the nozzle, which can be seen very clearly in Figure 10. Shock triple point is formed at the top and bottom end of the Mach disc followed by large scale coherent structures, shedding downstream periodically. Nozzle flow is inherently turbulent, as there are no flow quality control devices present in the stagnation chamber. But behind the Mach disc, as the flow is retarded to very low subsonic speed, flow becomes laminar. But around the triple point, flow is still turbulent and it is at supersonic speed. Hence, a laminar shear layer is formed initially, which then undergoes transition to turbulence. While undergoing transition, large scale structures

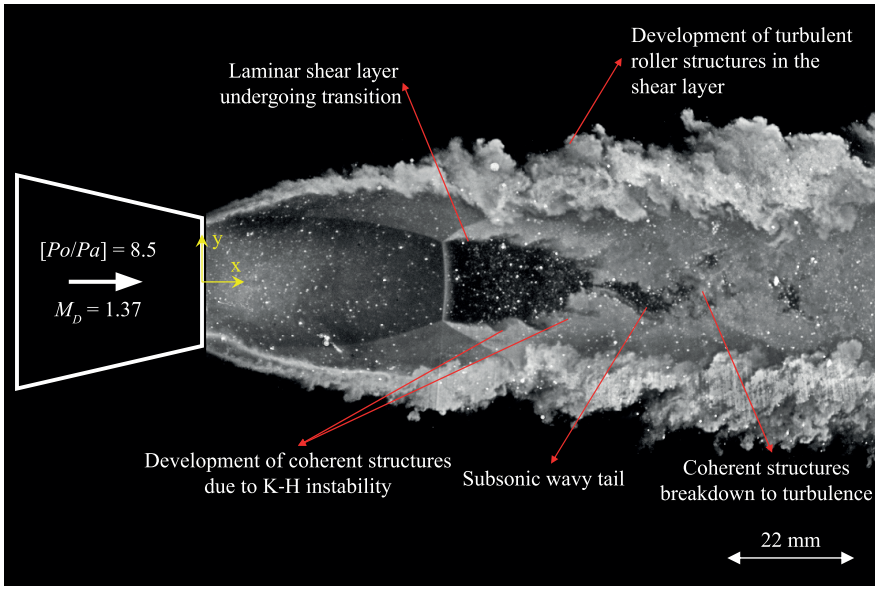

Figure 10: Instantaneous flow field of a supersonic axisymmetric free jet (conditions: P_o/P_a = 8.5, M_D = 1.37, moderate seeding).

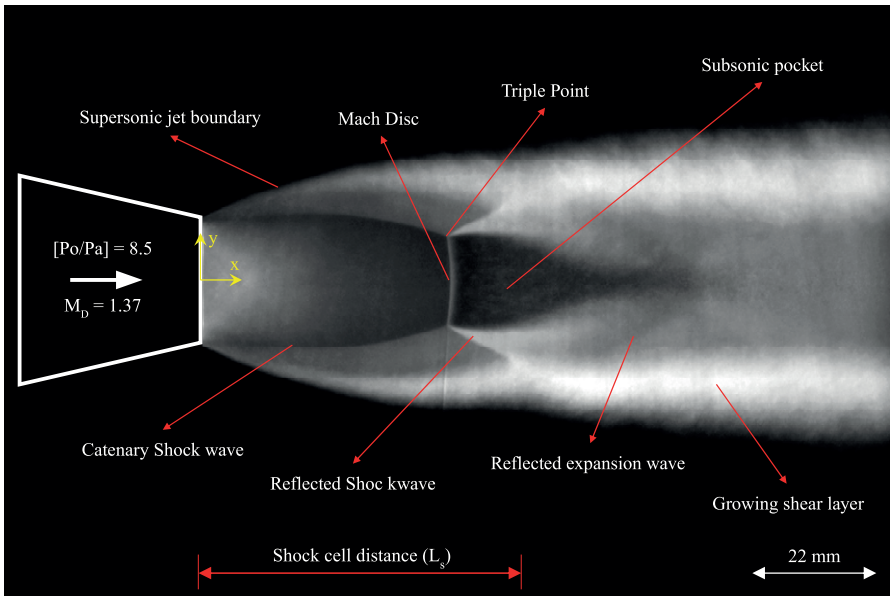

Figure 11: Time averaged flow field of a supersonic axisymmetric free jet (conditions: P_o/P_a = 8.5, M_D = 1.37, moderate seeding).

are produced, owing to K-H instability (Figure 10) in the interface of supersonic and subsonic flow. Shedding of such structures are crisply captured in PLMS imaging. Coming to the shear layer of the supersonic free jet itself, which looks like a twisting rope in Figure 10, one can see the thickening of the shear layer with a dilution in intensity downstream. It is a well-known fact that the free jet has a tendency to entrain the surrounding fluid in due course of propagation. This in-turn increases the effective jet width of the supersonic free jet along the flow direction. As the flow is continuously exchanging mass and momentum through shear layer, shear layer thickening happens (Figure 11) along the flow direction. Intensity dilution is happening as a by-product of mixing between two fluids having different densities. Series of non-correlated PLMS images at different time intervals are shown in Figure 12. Apart from the shedding of large scale structures near the triple point, unsteady oscillations of the subsonic wavy tail behind the Mach disc can be seen evidently in

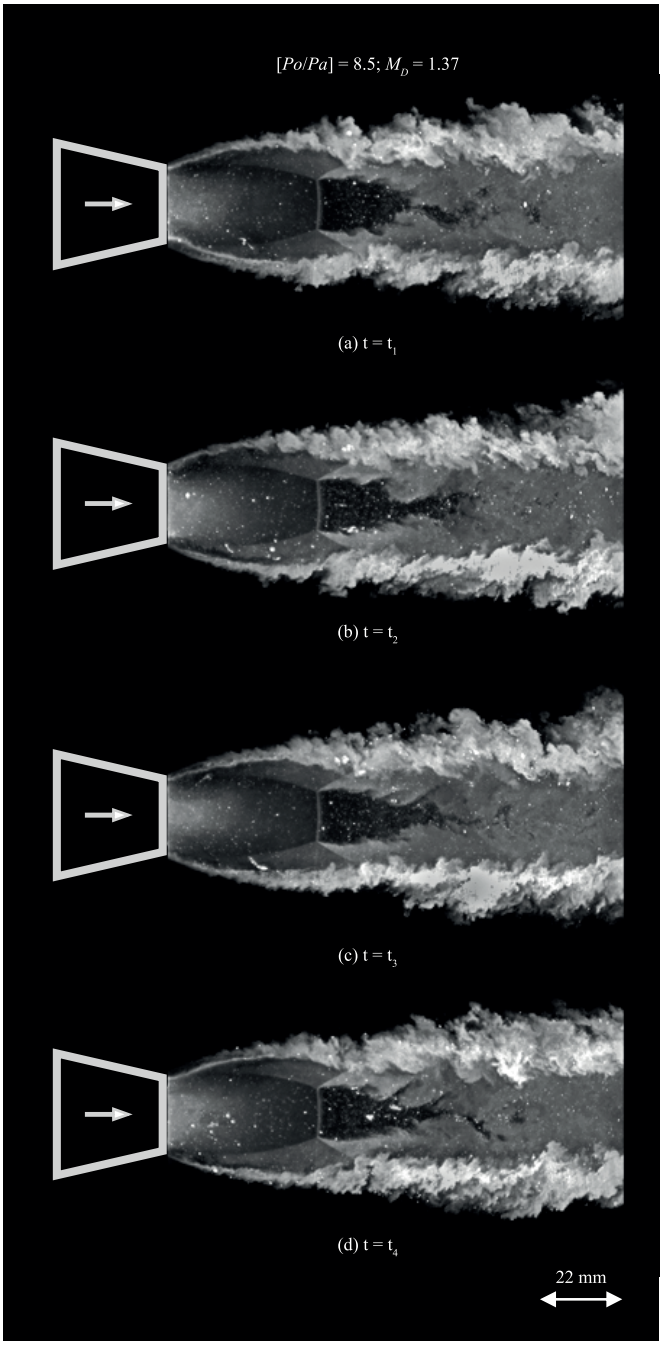

Figure 12: Instantaneous flow field of a supersonic axisymmetric free jet at different non-correlated time intervals showing the oscillations of the subsonic wavy tail (conditions: P_o/P_a = 8.5, M_D = 1.37, moderate seeding).

Figure 12. Subsonic wavy tail terminates around 2D from the Mach disc for the flow conditions under observation. Subsonic wavy tail oscillations are primarily due to the asymmetric interaction of those large scale shedding structures which breaks down to turbulent flow around the subsonic packet. Due to this rapid oscillation of subsonic wavy tail, flow across the triple point shear layer, mixes rapidly downstream. Then the mixed flow is accelerated to corresponding supersonic speed through multiple shocks (not shown in the presented image). It has to be noted that these multiple shocks are formed in the process of matching the jet pressure with atmospheric pressure, which are also oscillating with respect to time. Early literatures[42] have found out that these oscillations are one among the reason for the produced noise in a supersonic free jet.

3.1.2 Influence of design mach number and nozzle pressure ratio on a supersonic free jet: To study the influence of Design Mach number (M_D) and Nozzle Pressure Ratio (NPR) on a Supersonic Free jet, two conical nozzle of design Mach number 2.0 and 2.5 are considered. Flow through these nozzles are subjected to three different NPR of values 4.09, 7.39 and 8.09. Each of the NPR values correspond to a specific Fully Expanded Mach Number (M_J) of values 1.7, 2.0 and 2.1. Values of M_J can be obtained from Equation 1 as stated below. To see the influence of variations in Mach number and NPR together, M_R is defined as the ratio of M_D and M_J (Equation 2). Defined values of M_R helps in identifying the nozzle flow conditions. If the values of M_R are lesser than unity, then the nozzle is operating in under-expanded condition. If the values of M_R are greater than unity, then the nozzle is operating in over-expanded condition. Hence for the considered experiments, we will be achieving M_R of values 1.18, 1.0, 0.95, 1.47, 1.25 and 1.19.

$$M_J = \sqrt{\frac{2}{\gamma - 1}\left(NPR^{\frac{\gamma-1}{\gamma}} - 1 \right)} \quad (1)$$

$$M_R = \frac{M_D}{M_J} \quad (2)$$

Using an Nd-YLF laser at 0.8 kHz, PLMS images are captured for all the six values of M_R. Both instantaneous and time averaged PLMS images for M_D 2.0 & M_D 2.5 are shown in Figures 13 & 14, where the flow moves from left to right. Looking

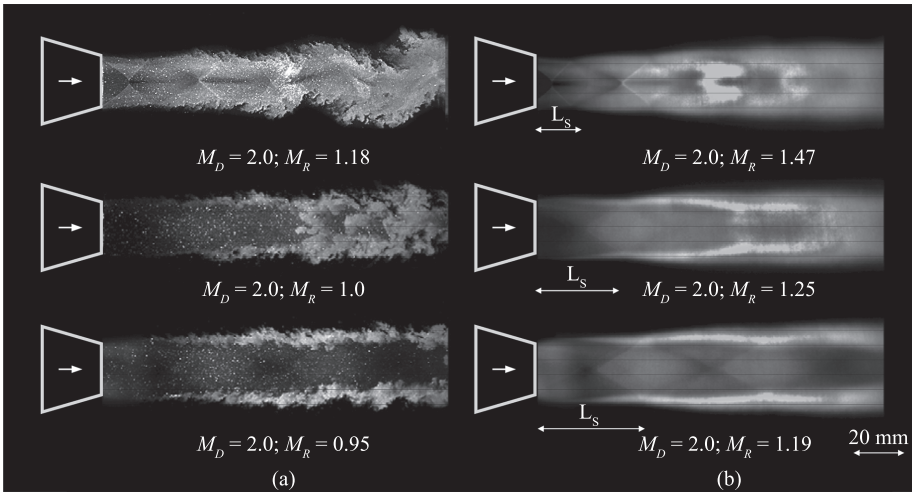

Figure 13: (a) Instantaneous and (b) time averaged flow field of a supersonic axisymmetric free jet (conditions: M_D = 2.0, moderate seeding).

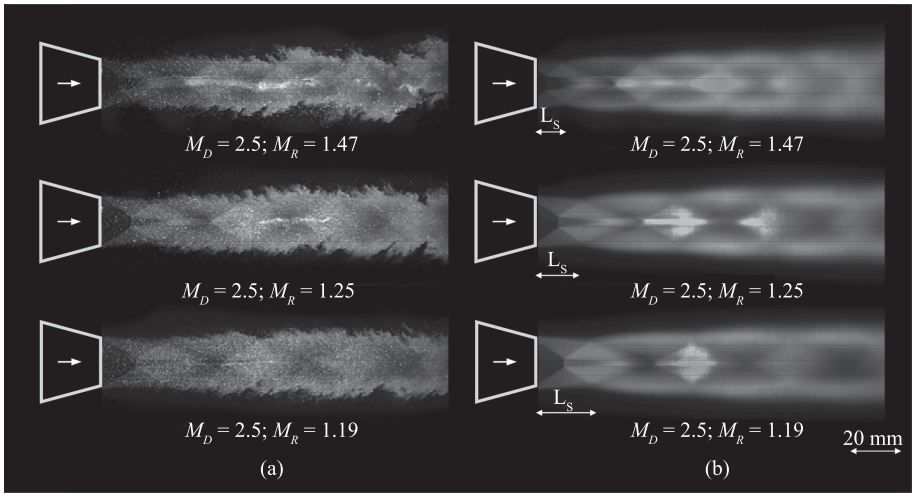

Figure 14: (a) Instantaneous and (b) time averaged flow field of a supersonic axisymmetric free jet (conditions: M_D = 2.5, moderate seeding).

at the image from top to bottom (decreasing M_R) in Figures 13(a) & 14(a), one can see the decaying strength of the wavy jet oscillation. Literature[43,44] identifies these wavy structures (sinuous) as modes of instability in a supersonic screeching jet. Screeching supersonic jets are observed when the nozzle is operating in over-expanded condition (M_R>1). Values of M_R at which a dominant screech frequency can be seen, varies for different M_D. For example, in our experiments, M_R of 1.18 for M_D = 2.0 and M_R of 1.47 for M_D = 2.5, produces higher amplitude wavy structures. When the values of M_R decreases towards unity or below unity, wavy jet oscillations are suppressed. In the case of M_R of 0.95 for M_D = 2.0, where the nozzle is operating in under-expanded condition, wavy structures are completely suppressed, though shock cells are visible. A notable case is M_R of unity for M_D = 2.0, where there are no visible strong shock structures unlike others. For almost perfectly expanded nozzle, this is expected as the static pressure of the jet and atmospheric pressure is merely matched. Instantaneous PLMS images reveal more such details. On looking at the time averaged PLMS images (nearly 800 images are used for time averaging), effective growth in jet width and increasing shock cell spacing can be seen. It is well established that the screeching jet produces enhanced mixing[45] and jet entrainment. Because of the asymmetric instability mode (wavy jet) associated with the screeching jet, effective jet width is found to be increasing. In Figure 15, several snap shots are taken at various time intervals, which show the convection of wavy structures produced in a screeching jet. Phase changes in wavy structures are marked by a yellow line that runs through the center of the jet column. These wavy structures increase the effective jet width, as

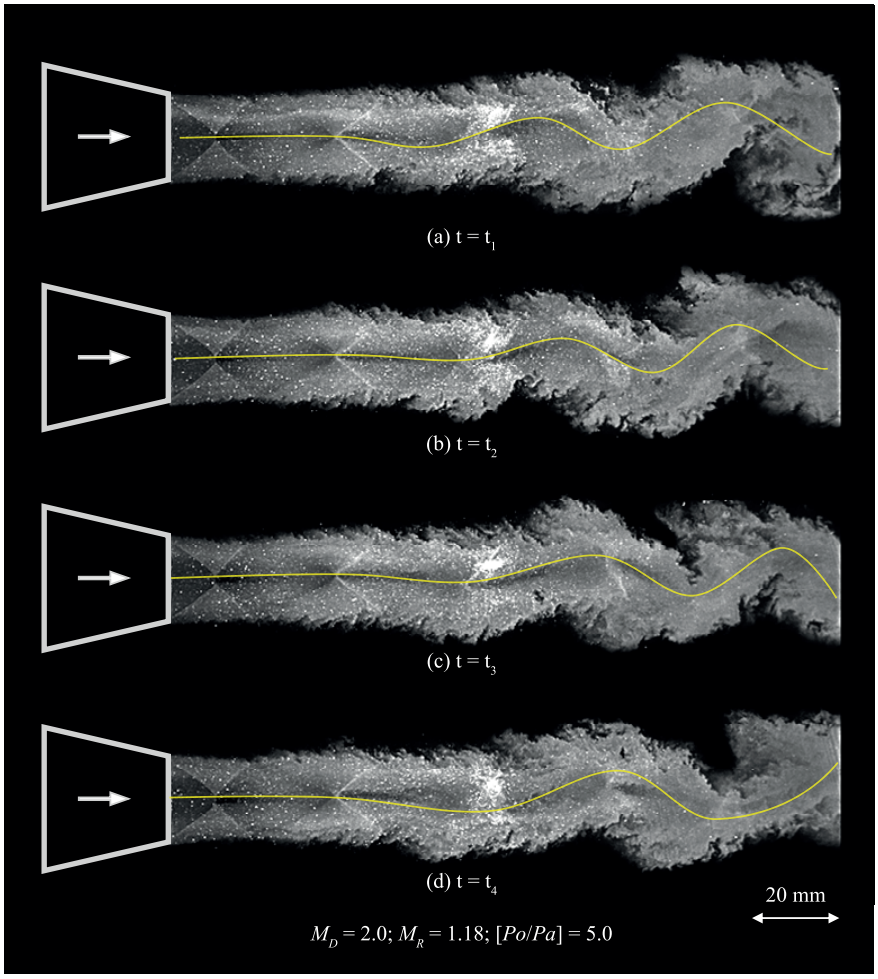

Figure 15: Instantaneous flow field of a screeching supersonic axisymmetric free jet at different non-correlated time intervals showing the jet flapping phenomena (conditions: P_o/P_a = 5.0, M_D = 2.0, M_R = 1.18; moderate seeding). Yellow line in the middle of the jet column shows the phase changes observed at different non-correlated time intervals.

this phenomenon is not seen in other operating conditions of the supersonic jet. Taking a vertical intensity scan in the time averaged PLMS images for different M_R at 6D downstream the nozzle exit, one can see that the wavy jets have more effective jet width. Out of all the six cases discussed here in this section, effective jet width is really larger (nearly 2D) for M_R of 1.18 at M_D = 2.0. Another interesting quantitative data that can be taken from the time averaged PLMS images is shock cell length (L_s). In Figure 13(b) & 14(b), one can clearly see the increase in the shock cell spacing as M_R decreases. Rapid rise in kinetic energy of the supersonic jet for decreasing M_R stands as one major reason for such behavior. Although for M_D = 2.0, such phenomena are difficult to appreciate visually, due to small barreling of shock cell structures, one can see the increasing shock cell length clearly for M_D = 2.5. Calculated values of shock cell spacing or effective jet width from time-averaged PLMS images are matching well with the empirical relationships that are reported in literatures. Detailed quantitative discussions of those are beyond the scope of current discussions and hence they are not included in this paper.

3.2 *Supersonic confined jet*

When the supersonic jet passes through an enclosed chamber, it is called as supersonic confined jet. They are extensively used in many engineering applications in the form of supersonic ejectors. Supersonic confined jets are visualized using PLMS imaging, by seeding the primary and secondary flow individually. Seeding of primary or secondary flow is important to bring out key flow structures that are observed in supersonic confined jets. For the current study, a primary supersonic jet of design Mach number (M_{PD}) 2.0 is achieved for three different primary flow stagnation pressure (P_{OP}) conditions, whose values are of 5.89 bar, 7.89 bar and 9.89 bar respectively. As the behavior of confined supersonic jets depend on various parameters, the observed values of vital parameters like Stagnation Pressure Ratio (SPR) and Entrainment Ratio (ER) must be mentioned. SPR is defined as the ratio of P_{OP} (primary flow stagnation pressure) and P_{OS} (secondary flow stagnation pressure), whereas ER is defined as the ratio of $\dot{m}_s$ (secondary mass flow rate) and $\dot{m}_p$ (primary mass flow rate). Basic flow features that are observed in a typical instantaneous and time-averaged PLMS images by seeding the primary flow and secondary flow individually are shown in Figures 16 and 17 (inverted images are presented here for better clarity). As the continuous jet entrainment process through the shear layer is restricted by the presence of walls, growth rate of the supersonic confined jets are smaller than the supersonic free jet. Large scale coherent structures are formed far downstream the nozzle, which later interact with the wall and break down. Turbulent mixing happens after the break down of such structures. These aspects are captured properly in Figure 16(a). In Figure 16(b), one can see the shock cell spacing (L_s) in the primary supersonic jet. While seeding the secondary flow, instability waves coming from the terminating primary flow potential core can be seen very clearly in Figure 17(a). Extent of the primary flow kinetic energy can be quantified by measuring the potential core length (L_{PC} or PCL) from the primary flow nozzle exit. Formation of distinct mixing layer (shear layer where primary and secondary flow diffuse through) can also be seen along with the shock cell boundary in Figure 17(b). In Figure 18, instantaneous and

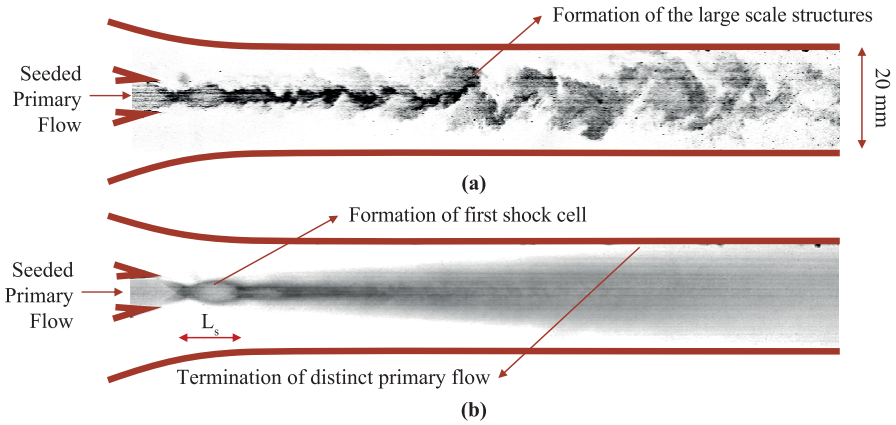

Figure 16: Typical (a) instantaneous and (b) time-averaged PLMS image obtained during the experiment by seeding the primary flow individually (conditions: MPD = 2.0, SPR = 7.09, ω = 0.46).

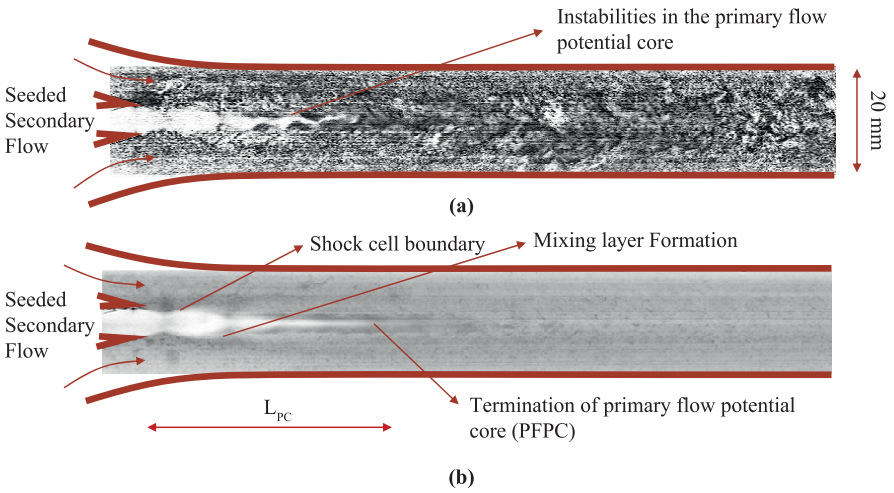

Figure 17: Typical (a) instantaneous and (b) time-averaged PLMS image obtained during the experiment by seeding the secondary flow individually (conditions: MPD = 2.0, SPR = 7.09, ω = 0.46).

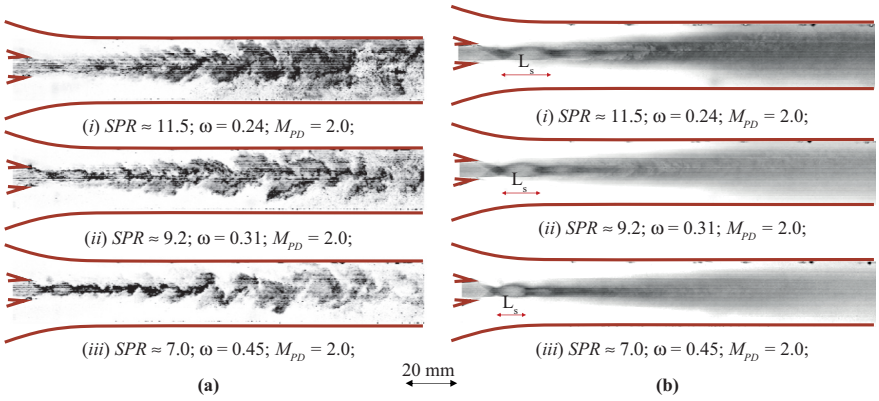

Figure 18: (a) Instantaneous and (b) time averaged flow field of a supersonic rectangular confined jet (conditions: M_{PD} = 2.0, moderate primary seeding).

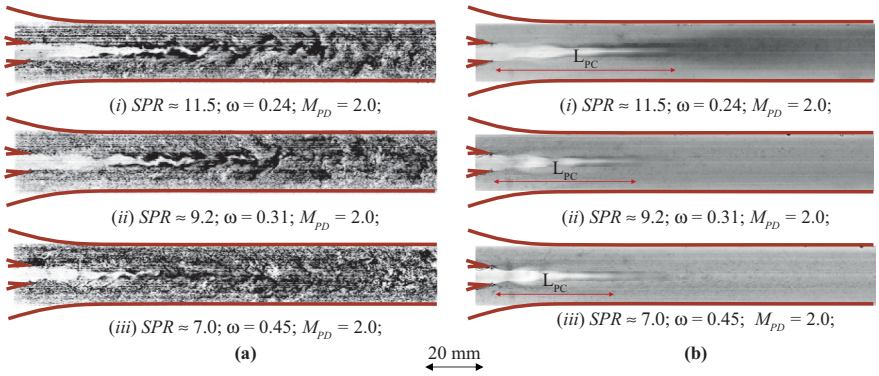

Figure 19: (a) Instantaneous and (b) time averaged flow field of a supersonic rectangular confined jet (conditions: M_{PD} = 2.0, moderate secondary seeding).

time-averaged PLMS images are taken for different SPR by seeding the primary flow. Thickness of the large scale coherent structures increases with increase in SPR, which can be seen evidently from Figure 18(a). This is primarily due to increase in the effective jet height (h_J) that corresponds to fully expanded primary flow Mach number (M_{PJ}) when P_{OP} (or SPR) increases. Values of h_J can be calculated using Equation 3, which is given below.

$$h_J = h\frac{M_{PD}}{M_{PJ}}\left[\frac{1+\frac{\gamma-1}{\gamma}M_{PJ}^2}{1+\frac{\gamma-1}{\gamma}M_{PD}^2}\right]^{\frac{\gamma+1}{2(\gamma-1)}} \quad (3)$$

Increase in shock cell spacing can also be seen clearly in Figure 18(b) when SPR increases. This is basically due to increase in M_{PJ}. In Figure 19, instantaneous and time-averaged PLMS images are taken for different SPR by seeding the primary flow. Increase in potential core length and increase in the wavelength of the potential core instability are observed for increasing SPR in Figure 19(a) and in Figure 19(b). Like the reason for the increment observed in L_s, increment in L_{PC} is also due to the rise in kinetic energy of the primary flow (or increase in M_{PJ}). Instabilities that are observed in the terminal region of the potential core is due to core turbulence effect[46] and self-sustained oscillation of the jet column.[44]

4 Conclusions

Visualization of supersonic free and confined jets are carried out using PLMS imaging technique in a blow-down facility established in LHSR, IISc – Bangalore. Particles for PLMS studies are selected, analyzed and produced using an in-house seeder to meet higher mass flow capabilities. A digital image processing routine is established to process the PLMS images. Supersonic axisymmetric free jet and supersonic planar (rectangular) confined jet are considered for these experiments. Following are the major flow features identified from PLMS imaging techniques:

i. Features like, jet shear layer, sinuous jet oscillations in screeching jet, growth in the effective jet width during screech, catenary shock, reflecting shock, Mach disc, K-H instability near the triple point, subsonic wavy tail and shock cell length variations are found in supersonic axisymmetric free jet. A qualitative variations in the effective jet width of a screeching jet and shock cell spacing in jets having different M_R are also highlighted.
ii. Features like mixing layer, jet column instability, terminal potential core instability, potential core length, shock cell boundary, shock cell length, thickness variations in large scale structures and turbulent break down of large scale structures are clearly seen in supersonic rectangular confined jet. A qualitative variations in the wavelength of the primary flow potential core instability and primary jet shock cell spacing with respect to SPR are discussed.

Acknowledgements

The authors would like to acknowledge the research grants from Defense Research and Development Organization (DRDO), India, towards this study. The authors are thankful to the members of the laboratory for their help during this study, especially Dr. Srisha, Mr. Albin, Dr. Bindu and Dr. Vikas. The authors are also grateful to Prof. D. Sivakumar and his students at Spray and Droplet Dynamics Laboratory, IISc, for helping out to use PDPA and Tesscorn Aerofluid Inc. for lending WRPS to measure particle sizes for PLMS studies.

Received 10 March 2016.

References

1. W. Merzkirch, *Flow Visualization*, Elsevier Science, (2012).
2. J.D. Bird, U.S.N. Aeronautics, S. Administration and L.R. Center, *Tuft-grid surveys at low speeds for delta wings*, National Aeronautics and Space Administration, (1968).
3. A.J. Smits, *Flow Visualization: Techniques and Examples*, Imperial College Press, (2012).
4. G.S. Settles, *Schlieren and Shadowgraph Techniques: Visualizing Phenomena in Transparent Media*, Springer-Verlag Berlin Heidelberg, (2001).
5. N.T. Clemens and M.G. Mungal, A Planar Mie Scattering Technique for Visualizing Supersonic Mixing Flows, *Exp. Fluids,* **11**, 175 (1991).
6. C.M. Fajardo, J.D. Smith and V. Sick, Sustained simultaneous high-speed imaging of scalar and velocity fields using a single laser, *Appl Phys B-Lasers* O, **85**, 25 (2006).
7. Z.P. Berger, P.R. Shea, M.G. Berry, B.R. Noack, S. Gogineni and M.N. Glauser, Active Flow Control for High Speed Jets with Large Window PIV, *Flow Turbul Combust,* **94**, 97 (2015).
8. H. Takahashi, M. Hirota, H. Oso and G. Masuya, Measurement of Supersonic Injection Flowfield Using Acetone PLIF, *T Jpn Soc Aeronaut S,* **51**, 252 (2009).
9. N.T. Clemens and M.G. Mungal, 2-Dimensional and 3-Dimensional Effects in the Supersonic Mixing Layer, *AIAA J.*, **30**, 973 (1992).
10. T.C. Island, B.J. Patrie, M.G. Mungal and R.K. Hanson, Instantaneous three-dimensional flow visualization of a supersonic mixing layer, *Exp. Fluids,* **20**, 249 (1996).
11. N.T. Clemens and M.G. Mungal, Large-Scale Structure and Entrainment in the Supersonic Mixing Layer, *J. Fluid Mech., 2***84**, 171 (1995).
12. D.R. Eklund, S.D. Stouffer and G.B. Northam, Study of a supersonic combustor employing swept ramp fuel injectors, *J. Propul. Power,* **13**, 697 (1997).
13. M. Hirota, S. Koike, K. Tanaka, K. Takita and G. Masuya, PIV measurement of single-port and twin-port injection in supersonic flow, ICIASF '05 Record: 21 st International Congress on Instrumentation in Aerospace Simulation Facilities 330, (2005).

14. T. Sunami and F. Scheel, Observation of mixing and combustion processes of H-2 jet injected into supersonic streamwise vortices, *Shock Waves*, Vols 1 and 2, Proceedings 921, (2005).
15. S. Sujith, T.M. Muruganandam and J. Kurian, Effect of Trailing Ramp Angles in Strut-Based Injection in Supersonic Flow, *J. Propul. Power,* **29**, 66 (2013).
16. C. Aguilera and K.H. Yu, Supersonic Mixing Enhancement Using Fin-Guided Fuel Injection, *J. Propul. Power,* **31**, 1532 (2015).
17. K.H. Yu, R.A. Smith, K.J. Wilson and K.C. Schadow, Effect of excitation on supersonic jet afterburning, *Combust. Sci. Technol.,* **113**, 597 (1996).
18. K.H. Yu, K.C. Schadow, K.J. Kraeutle and E.J. Gutmark, Supersonic-Flow Mixing and Combustion Using Ramp Nozzle, *J. Propul. Power,* **11**, 1147 (1995).
19. Y. Haimovitch, E. Gartenberg, A.S. Roberts and G.B. Northam, Effects of internal nozzle geometry on compression-ramp mixing in supersonic flow, *AIAA J.*, **35**, 663 (1997).
20. N.M. Sijtsema, R.A.L. Tolboom, N.J. Dam and J.J. ter Meulen, Two-dimensional multispecies imaging of a supersonic nozzle flow, *Opt. Lett*., **24**, 664 (1999).
21. R. Ramesh, S. Pradeep, T.M. Muruganandam and R.I. Sujith, Studies on freejets from nozzles for high-speed mixing applications, *Exp. Fluids,* **29**, 359 (2000).
22. R.I. Sujith, R. Ramesh, S. Pradeep, S. Sriram and T.M. Muruganandam, Mixing of high speed coaxial jets, *Exp. Fluids,* **30**, 339 (2001).
23. J.C. Hermanson and M. Winter, Mie Scattering Imaging of a Transverse, Sonic Jet in Supersonic-Flow, *AIAA J*., **31**, 129 (1993).
24. M.R. Gruber, A.S. Nejad, T.H. Chen and J.C. Dutton, Mixing and Penetration Studies of Sonic Jets in a Mach-2 Freestream, *J. Propul. Power,* **11**, 315 (1995).
25. M.R. Gruber, A.S. Nejad, T.H. Chen and J.C. Dutton, Compressibility effects in supersonic transverse injection flowfields, *Phys. Fluids,* **9**, 1448 (1997).
26. M.R. Gruber, A.S. Nejad, T.H. Chen and J.C. Dutton, Transverse injection from circular and elliptic nozzles into a supersonic crossflow, *J. Propul. Power,* **16**, 449 (2000).
27. S. Murugappan, E. Gutmark, C. Carter, J. Donbar, M. Gruber and K.Y. Hsu, Transverse supersonic controlled swirling jet in a supersonic cross stream, *AIAA J*., **44**, 290 (2006).
28. J.A. Boles, J.R. Edwards and R.A. Baurle, Large-Eddy/Reynolds-Averaged Navier-Stokes Simulations of Sonic Injection into Mach 2 Crossflow, *AIAA J*., **48**, 1444 (2010).
29. J.C. Hermanson and B.M. Cetegen, Mixing enhancement of non-uniform density turbulent jets interacting with normal shock waves, Twenty-Seventh Symposium (International) on Combustion, 1–2, 2047 (1998).
30. U. Brummund and B. Mesnier, *A comparative study of planar Mie and Rayleigh scattering for supersonic flowfield diagnostics*, Iciasf'99: International Congress on Instrumentation in Aerospace Simulation Facilities, Record 421, (1999).
31. C.J. Bourdon and J.C. Dutton, Altering turbulence in compressible base flow using axisymmetric sub-boundary-layer disturbances, *AIAA J*., **40**, 2217 (2002).
32. S.M.V. Rao and G. Jagadeesh, Novel supersonic nozzles for mixing enhancement in supersonic ejectors, *Appl. Therm. Engg.*, **71**, 62 (2014).
33. M. Vishwakarma and A. Vaidyanathan, Experimental study of mixing enhancement using pylon in supersonic flow, *Acta Astronaut.,* **118**, 21 (2016).
34. S.M.V. Rao, *Experimental investigation on supersonic ejectors*, Ph.D. thesis, Indian Institute of Science, Bangalore, India, (2013).
35. S.M.V. Rao and G. Jagadeesh, Visualization and image processing of compressible flow in a supersonic gaseous ejector, *Journal of Indian Institute of Science,* **93**, 57 (2013).
36. S.M.V. Rao and G. Jagadeesh, Observations on the non-mixed length and unsteady shock motion in a two dimensional supersonic ejector, *Phys. Fluids,* **26**, (2014).
37. S.K. Karthick, S.M.V. Rao, G. Jagadeesh and K.P.J. Reddy, *Visualizing the flow through a supersonic gaseous ejector using Planar Laser Mie Scattering*: *10th Pacific Symposium on Flow Visualization and Image Processing*, Naples, Italy, 15–18, June, 2015, 8.
38. P. Desevaux, A. Mellal and A. de Sousa, Visualization of secondary flow choking phenomena in a supersonic air ejector, *J. Visualization,* **7**, 249 (2004).
39. T. Marynowski, P. Desevaux and Y. Mercadier, Experimental and Numerical Visualizations of Condensation Process in a Supersonic Ejector, *J. Visualization* **12**, 251 (2009).
40. A. Bouhanguel, P. Desevaux and E. Gavignet, Flow visualization in supersonic ejectors using laser tomography techniques, *Int. J. Refrig*., **34**, 1633 (2011).
41. A. Bouhanguel, P. Desevaux and E. Gavignet, Visualization of flow instabilities in supersonic ejectors using Large Eddy Simulation, *J. Visualization,* **18**, 17 (2015).
42. C.K.W. Tam, Supersonic Jet Noise, *Annu. Rev. Fluid Mech., 2***7**, 17 (1995).
43. C.A. Shih, A. Krothapalli and S. Gogineni, Experimental-Observations of Instability Modes in a Rectangular Jet, *AIAA J.,* **30**, 2388 (1992).
44. D. Moreno, A. Krothapalli, M.B. Alkislar and L.M. Lourenco, Low-dimensional model of a supersonic rectangular jet, *Phys. Rev. E*., **69**, (2004).
45. A. Krothapalli and Y.C. Hsia, Discrete tones generated by a supersonic jet ejector, *J Acoust Soc Am,* **99**, 777 (1996).
46. G. Raman and E.J. Rice, *Core turbulence effect on naturally occuring modes in a circular jet*, Springer Netherlands, (1993).

S.K. Karthick is currently pursuing his doctoral studies in the Department of Aerospace Engineering, IISc, Bangalore. He is currently working on the aspects of flow physics involved in the mixing process inside a supersonic ejector (supersonic jet in confinement). He has also been involved in the studies on supersonic projectiles in ground proximity, auto-rotating seeds, plasma flow control, human breathing, shock tunnel investigations and mixing enhancement in supersonic free jets. His areas of interest include high speed flows, high speed imaging and processing, supersonic mixing and advanced optical flow diagnostics like PLMS, PIV & PLIF. He has published 9 conference papers. He finished his post-graduation in Space Engineering and Rocketry from BIT, Mesra.

G. Jagadeesh is a Professor in the Dept. of Aerospace Engineering, IISc, Bangalore. He is fellow of Indian National Academy of Engineering and an Associate fellow of American Institute of Aeronautics and Astronautics. He is professionally associated with International Shock Wave Institute & Society for Shock Wave Research, India. He is Presently working on Hypersonic flow control using novel energy deposition methods; Supersonic mixing enhancement in ejectors; Shockwave propagation dynamics in complex fluids; New automated wave reactors for industrial and biomedical applications. His areas of interest include Experimental Hypersonic, Shock wave dynamics. He has published over 150 scientific papers in International journals and symposiums. He has completed his PhD from IISc Bangalore.

K.P.J. Reddy received his Ph.D. degree in 1981. He joined the department of Aerospace Engineering, IISc in 1981. He has held many positions since, and currently he is holding the post of Senior Professor. He has published over 200 scientific papers in International journals and symposiums. Prof. Reddy is the founder President of Society for Shock Wave Research, India and also the President of International Shock Wave Institute at Nagoya, Japan. He recently received Honor Diploma from Minsk International Forum on Heat and Mass Transfer, Minsk, Belarus and IISc Alumni Award for Excellence in Engineering Research in 2010. At present he is Prof. Satish Dhawan ISRO Chair Professor in the Department of Aerospace Engineering. He is also an Adjunct Professor of the Defense Institute of Advanced Technology, Pune.